Volkson Press

Journal of Water Resources (JWR)

DOI: http://doi.org/10.7508/jwr.01.2023.01.09

ISSN: 2327-7262 (Print)
ISSN: 2327-7688 (Online)
CODEN : JWROB9

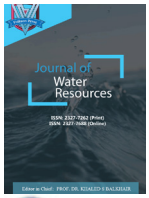

CrossMark

ARTICLE

COMPARATIVE STUDY OF MESOSCALE EDDIES IN THE NORTHWEST PACIFIC OCEAN

Dehou Yang[1],Yuejin Li[1,2], Huayong Yang[1*]

[1]Southern Marine Science and Engineering Guangdong Laboratory (Guangzhou), Guangzhou 511458, China
[2]School of Electromechanical Engineering, Guangdong University of Technology, Guangzhou 510006, China
[*]Corresponding Author E-mail: E-mail：yanghy@ gmlab.ac.cn

ARTICLE DETAILS

Article History:

Received 8 January 2023
Accepted 15 February 2023
Available online 1 March 2023

ABSTRACT

In this paper, satellite remote sensing data are used to study two typical sea areas in the Northwest Pacific: The eddy in Kuroshio Extension (KE) and Subtropical Counter current (STCC) is statistically analyzed, including its basic characteristics, spatial distribution and propagation characteristics, and its seasonal and interannual variations are analyzed. Through comparison, it is found that the eddy characteristics of the two sea areas are quite different. Instead of keeping data such as Argo (Array for Real-time G-costrophic Oceanography), the vertical structure characteristics of eddies in the two sea areas (zone A and Zone B) were analyzed and compared. The results show that the potential temperature anomaly and salinity anomaly of the eddies in area A are smaller than those in area B, which presents opposite characteristics to the potential density anomaly.

KEYWORDS

North pacific, Kuroshio extension, subtropical counter current, eddy.

1. INTRODUCTION

Mesoscale eddies exists widely in the ocean, with a horizontal scale of about 100-500 km and a life cycle of about 20-200 d, moving at a speed of (1-5) ×10-2 m/s [1]. In the northern hemisphere, under the action of Coriolis force, the water on the surface of the sea diverges outwards, and the height of the sea surface is a negative anomaly. In addition, vertical upward water movement is formed in the center of the eddy, which cools the internal water, so it is called cold eddy. On the contrary, for the counter-gas eddy rotating clockwise, the sea surface height is positive anomaly and the internal water body is warmed, which is called warm eddy [2]. Mesoscale eddies are nonlinear and isolated, trapping seawater and spreading westward, which can affect the transport of material [3,4]. As a significant ocean phenomenon, mesoscale vorticity has a maximum vertical influence depth of several thousand meters [5]. The motion of mesoscale vorticity usually carries huge kinetic energy, accounting for 80% of the kinetic energy of ocean circulation [3], which is an order of magnitude or larger than the average current [2], and is an important component of ocean dynamics [6,7]. Therefore, it plays an important role in regulating ocean circulation and affecting temperature, salinity and chlorophyll distribution [8-14].

With the launch of Topex/Poseidon satellite in 1992, people can rely on the ocean circulation and sea surface height field data obtained by the satellite to identify and observe mesoscale eddies. The circulation in the North Pacific Ocean is complex and the mesoscale eddy is very frequent. Therefore, it is very important to understand the motion and characteristics of the mesoscale eddy in the North Pacific Ocean for the understanding of global climate change and air-sea interaction. It is generally believed that the areas with frequent mesoscale eddy activities in the North Pacific are the Kuroshio Extended body area (KE) and subtropical countercurrent area (STCC), which are the two latitudinal belts of high eddy kinetic energy in the North Pacific [15]. KE is a current system with large amplitude meandering and a large number of high-energy eddies [16], while a large number of mesoscale eddies exist in the STCC sea area, which are constantly enhanced during the westward movement and exert an impact on the Kuroshio [17]. Therefore, the study of mesoscale eddies in KE and STCC, two typical sea areas in the North Pacific, is of great scientific significance for understanding the characteristics of mesoscale eddies in the North Pacific and the multi-spatio-temporal scale variations of sea circulation.

Based on satellite altimeter data, many studies have been conducted on mesoscale eddies in the ocean. For KE area, Ebuchi and Hanawa (2001) used SLA (Sea Level Anomaly) data to extract and screen the recirculating eddies south of Kuroshio extension and nearby mesoscale eddy, and found that the submarine topography has an impact on the movement and extinction of mesoscale eddy [18]. Sasaki and Minobe (2015) proposed a method to track the eddies in the sea area through changes in the length of the current axis of the Kuroshio extension body, and analyzed the interannual variation of the number of mesoscale eddies in the upper and lower reaches of the Kuroshio extension body and its mechanism [19]. Ding et al. (2019) used the fusion data of AVISO satellite altimeter from 1993 to 2015 to make a statistical analysis of the spatial distribution characteristics, movement attributes and seasonal, interannual and decadal changes of the shedding eddies from the flow axis of the extended Kuroshio body, and described in detail the relationship between the interannual to decadal changes in the formation of shedding eddies and the KE state [20]. For STCC sea area, Qiu (1999) analyzed 5 years of TOPEX/Poseidon (October 1992 - December 1997) satellite altimeter data, focusing on STCC sea area in the North Pacific Ocean, and found that its eddy energy could reach half of the Kuroshio extension

body, and the eddy energy had a clear annual period [21]. Qiu and Chen (2014) compared seasonal STCC changes in mesoscale and subscale using high-resolution OGCM simulation and satellite altimeter data, and concluded that there were seasonal variations in root mean square values of STCC eddy kinetic energy and vorticity [22]. Li (2017) used 23 years' satellite altimeter data and WOA18 climate state monthly mean temperature and salinity data to investigate the eddy kinetic energy spectrum and its dynamic process of eddy scale seasonal variation in STCC sea area, and found that the baroclinic instability caused by the seasonal variation of ocean stratification and geostrophic vertical shear is related to the seasonal variation of eddy kinetic energy spectrum [23].

It can be seen that scholars have done a lot of research on mesoscale eddies in STCC and KE sea areas, but most of them are limited to their respective sea areas, and few scholars have conducted comparison and research on the two sea areas in the same period. Chelton et al. (2011) studied the mesoscale eddies in the global waters [3], but the study was too large to accurately reflect the characteristics of the eddies in various waters of the North Pacific. Therefore, in order to solve the above problems, we used the alter fusion data from 1993 to 2020 to track and identify the mesoscale eddies in two typical sea areas (KE sea area and STCC sea area) in the Northwest Pacific Ocean, and statistically, analyzed and compared the characteristics of the eddies as well as the seasonal and interannual variations of the two sea areas, and synthesized and compared the vertical structure of the eddies, in order to further understand the characteristics of the eddies in the two sea areas.

2. DATA AND METHOD

2.1 Satellite Altimeter Data

The data for mesoscale eddy feature analysis come from a set of daily SLA data released by AVISO (Archiving Validation and Interpretation of Satellite Oceanographic). A mesoscale eddy data product using a novel vortex recognition algorithm. The data product covers the period from January 1, 1993 to May 17, 2020, including the location (longitude and latitude), life cycle, eddy radius, eddy amplitude and rotation speed of mesoscale eddies. The data period is from January 1, 1993 to January 1, 2018. Delayed Time (DT) data is obtained, and after January 1, 2018, Near Real Time (NRT) data is obtained. The parameter variables provided by NRT are more than DT, and the minimum life cycle of the eddy identified by DT is 28 days. The minimum life cycle of the eddy identified by NRT is 14 days.

2.2 Argo Floats Data

The International Argo program began in earnest in 2000. The Argo Global Project, a collaboration of more than 30 countries, including the United States, France and Japan, makes up for altimeters' inability to observe deep ocean data. Currently, the number of Argo drifting buoys worldwide is approximately 3900 (Figure 1). When Argo is working in the ocean, it will dive to a depth of 1,000 meters, float with the sea for about nine days, and then descend to a set maximum depth of 2,000 meters. It will automatically float up, and observe the temperature, salinity and pressure of the ocean during the rising process. When the floating buoy rises to the surface of the sea, The observation data and position will be transmitted by satellite to the ground station.

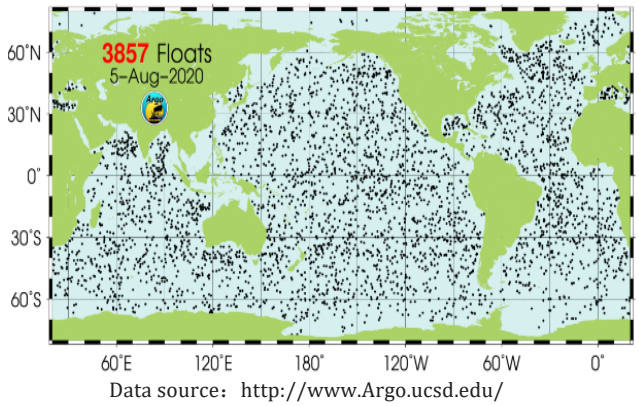

Data source：http://www.Argo.ucsd.edu/

Figure 1: Argo buoy global position

3. STUDIES ON MESOSCALE EDDIES IN THE NORTHWEST PACIFIC OCEAN

Figure 2 shows the average distribution of EKE in the North Pacific during the last 26 years (1993-2018). Large EKE is found in the central and western parts of the North Pacific Ocean. In order to compare and explore the characteristics of eddies in STCC and KE, STCC [Area A (120-180°E, 20-30°N) in Figure 2] and KE [Area B (142-180°E, 30-40°N) in Figure 2] are selected. Satellite remote sensing data are used to analyze the attributes and distribution characteristics of eddies in the selected area. The seasonal and interannual variations were studied, and the vertical structure of the eddies in the sea area (zone A and Zone B) was synthesized, analyzed and compared by combining Argo data.

3.1 Basic Characteristics

Based on AVISO's eddy data set, this paper first analyzes the characteristics of the number, average life cycle, average amplitude, average radius and average rotation velocity of different eddy types in different areas of the Northwest Pacific Ocean during 1993-2020 (Table 1). In the study area from 1993 to 2020, 14,875 eddies were generated in the recent 28 years. The number of eddies generated in area a (cyclonic eddy and anti-cyclonic eddy) was greater than that in area B, and the number of anti-cyclonic eddies generated in both areas was smaller than that of gas eddies. The average life cycle of the eddies in area A is smaller than that in area B, and the average amplitude of the eddies in area B is almost twice that in area A. The eddies in area A and area B have little difference in radius, but the average radius of cyclonic eddies in the two areas is smaller than that of anti-cyclonic eddies. The rotation speed of the eddy in area B is greater than that in area A.

The overall statistical characteristics of eddies obtained above are basically consistent with the results of previous studies. However, due to the differences in the data used, the sea area studied and the life cycle range of the selected eddies, there are some numerical differences in the characteristics of some eddies. For example, in the sea area A, the average radius of the eddies is slightly larger than the results studied by Liu et al. (2012) (the average radius of the cyclonic eddy is 84.7 km, and the anti-cyclonic eddy is 86.2 km) [24], and the life cycle of the eddies is also smaller than the results of previous studies (about 18 weeks). The sea area selected by Liu et al. (2012) was 15°-28°N and 115°E-150°W, and the life cycle of the selected eddies was more than 8 weeks[24]. Therefore, the selection of different sea areas and the selection of different life cycle ranges of the eddies will affect the performance of the characteristics of the eddies to a certain extent.

Figure 3 (a) shows the columnar distribution of the number of eddies in different life cycle ranges for the eddies whose life cycle is longer than 4 weeks. Generally speaking, the number of eddies produced in area A is greater than that in area B in each life cycle range. Table 2 statistics the number and proportion of eddies in each life cycle range in area A and Area B. According to the calculation, the number of eddies with A life cycle of less than 100 days in area A and B accounted for 76.40% and 70.62% of the total number, respectively, while the number of eddies with a longer life cycle (more than 100 days) accounted for 23.60% and 29.38% of the total number. It can be seen that eddies with a life cycle of less than 100 days are dominant in the sea area. Figure 3 (b) shows the spatial distribution of the number of eddies generated. The number of mesoscale eddies generated in area A (120-180°E, 20-30°N) is larger than that in area B (142-180°E, 30-40°N).

Figure 4 shows the moving track of long-period mesoscale eddies (over 45 cycles) in the study area (zones A and B). Apparently, most eddies travel from east to west. Figure 5 shows the frequency distribution of westward propagating eddies moving towards the equator and poleward in the study area (zones A and B) (cyclonic eddies in blue and anti-cyclonic eddies in red). In the latitudinal direction, due to the β effect, the mesoscale eddies in the North Pacific mainly moves westward. In area A, during the westward movement of the eddies, the cyclonic eddies and anti-cyclonic eddies moving towards the equator accounted for 55.36% and 54.62% of the total, respectively, while in area B, they

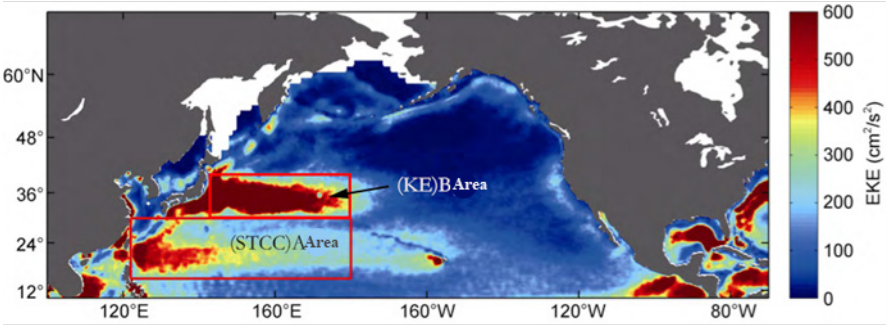

Figure 2: Distribution of Eddy Kinetic Energy (EKE) of mesoscale eddies in the North Pacific from 1993 to 2018[87]

Table 1: Statistical characteristics of eddies over parts of the Northwest Pacific during 1993-2020

Sea area	Type	Quantity	Average life cycle (day)	Average amplitude (cm)	Mean radius (km)	Average rotation speed (cm/s)
A	cyclonic eddy	4909	62	8	90	24
	anti-cyclonic eddy	4496	65	8	93	24
A	cyclonic eddy	2784	78	16	85	38
	anti-cyclonic eddy	2686	75	15	91	34

were 58.41% and 51.14%, indicating that both the cyclonic eddies and anti-cyclonic eddies had a tendency to drift towards the equator and the polar regions during the westward movement. In the study area (area A and area B), the probability of the eddy moving towards the equator is greater than that towards the pole, and the range of the polar movement and the equatorial movement is almost concentrated within 2°.

In area A, the average longitude of cyclonic eddies and anti-cyclonic eddies moving westward is 3.95° and 4.14°, In area A, the average longitude of cyclonic eddies and anti-cyclonic eddies moving westward is 3.95° and 4.14°, and 2.80° and 2.35° in area B. Longitudinally, And 2.80° and 2.35° in area b. Longitudinally, the average latitudes of the cyclonic eddies and anti-cyclonic eddies moving towards the equatorial direction and the polar direction are 0.95° and 0.76°, 0.92° and 0.77°, and 0.89° and 0.75°, Direction are 0.95° and 0.76°, 0.92° and 0.77°, and 0.89° and 0.75°, 0.74° and 0.73° in the sea area of B. It can be found that the average longitude of cyclonic eddies and anti-cyclonic eddies. 0.74° and 0.73° in the sea area of b. It can be found that the average longitude of gas cyclonic eddies and anti-cyclonic eddies moving westward in area A is larger than that in area B, and the average latitude of equatorial or polar movement is larger than that in area B. In area A, the average longitude of cyclonic eddies and anti-cyclonic eddies moving westward is 3.95° and 4.14°, and 2.80° and 2.35° in area B. Longitudinally, the average latitudes of the cyclonic eddies and anti-cyclonic eddies moving towards the equatorial direction and the polar direction are 0.95° and 0.76°, 0.92° and 0.77°, and 0.89° and 0.75°, 0.74° and 0.73° in the sea area of B. It can be found that the average longitude of cyclonic eddies and anti-cyclonic eddies moving westward in area A is larger than that in area B, and the average latitude of equatorial or polar movement is larger than that in area B.

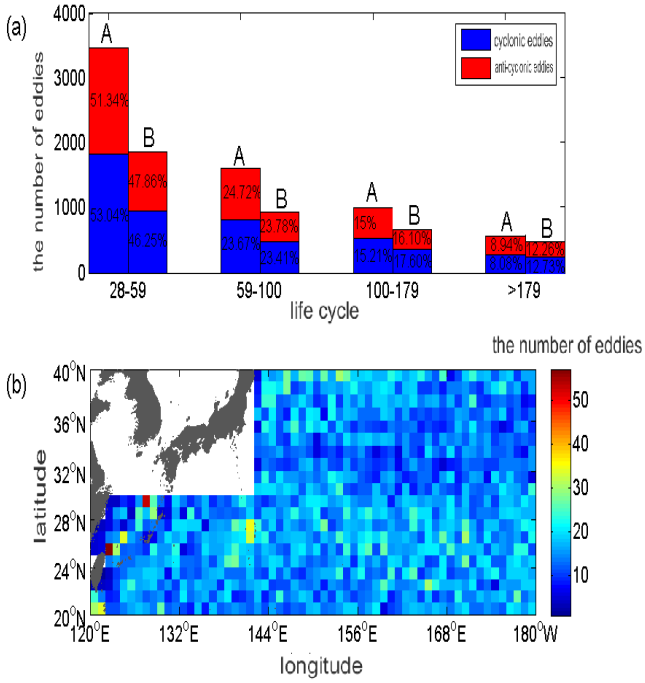

Figure 3: The statistics of the number of eddies in different life period (a) and the spatial distribution of the number of eddies (b)

Table 2: The number and proportion of eddies in each life period range of area A and area B

Life cycle (days)	28-59	59-89	100-179	>179
Area A sea area	3474/52.22%	1608/24.17%	1005/15.11%	565/8.49%
Area B sea area	1948/47.03%	977/23.59%	699/17.18%	518/9.63%

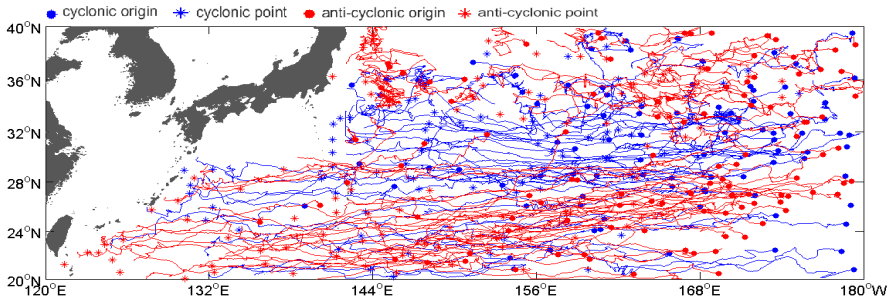

Figure 4: The moving track of long period mesoscale eddies (more than 45 cycles)

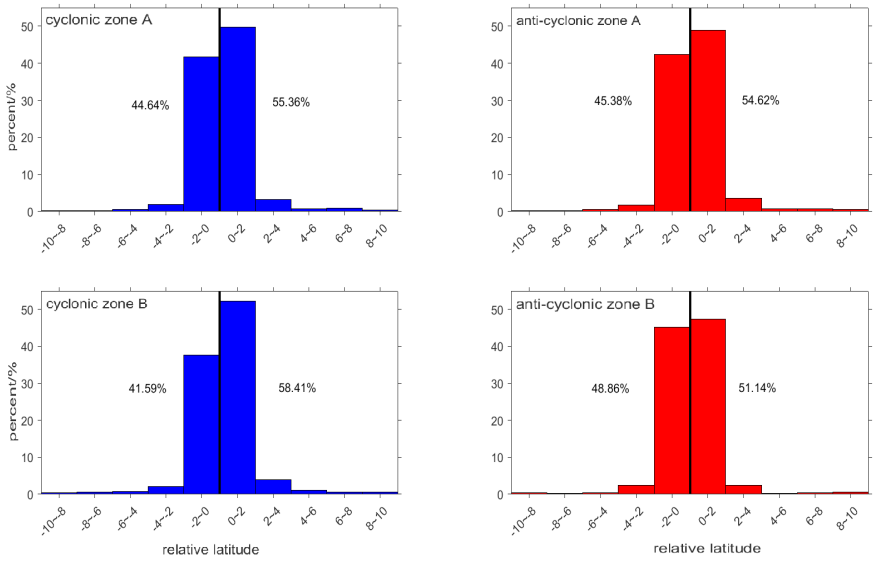

Figure 5: The frequency distribution of westward propagating eddies in the equatorial and poleward directions

(Blue is cyclonic eddy, red is anti-cyclonic eddy)

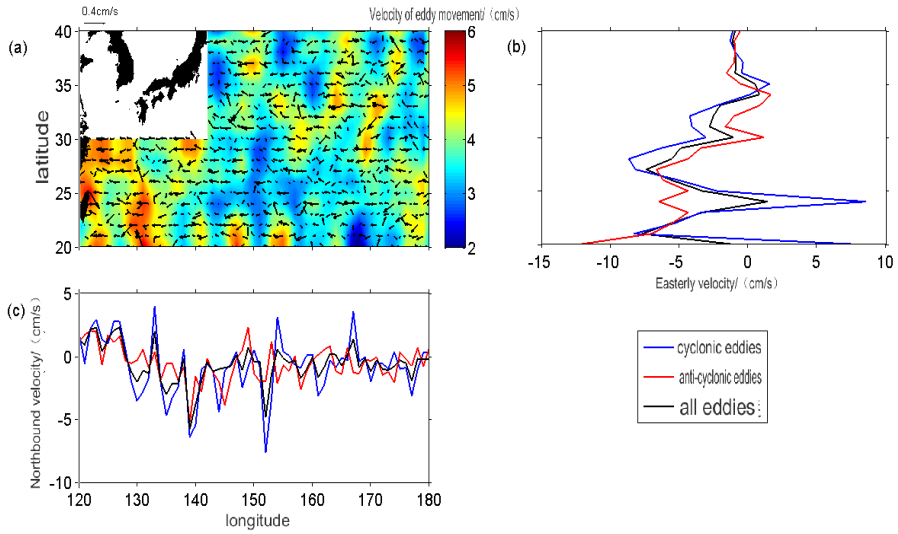

Figure 6: Vector field of mesoscale eddy-propagating motion (a), zonal mean velocity (b), and meridional mean velocity (c)

The eddies is influenced by the background flow field and β effect. The propagation velocity of mesoscale eddies in the study area (area A and area B) was quantitatively analyzed, and the propagation characteristics (Figure 6 (a)), the zonal average (Figure 6 (b)) and the meridional average movement velocity distribution (Figure 6 (c)) of the eddies in part of the Northwest Pacific Ocean were obtained. According to Figure 6 (b), most eddies in the study area propagate westward, which is consistent with the conclusion drawn in Figure 4. As can be seen from Figure 6 (b) and 6 (c), the velocity component of westward propagation at low latitude (20-30°N) is greater than that at high latitude (30-40°N). The eddies mainly propagates in the southwest direction in the study area. There is no significant difference between the propagation velocity of cyclonic eddies and anti-cyclonic eddies in longitude direction. In latitude direction, at about 24°N, the eastward propagation velocity of cyclonic eddies are close to 10 cm/s, while the anti-cyclonic eddies are westward propagation.

Figure 7 shows the spatial distribution of amplitudes and radii of

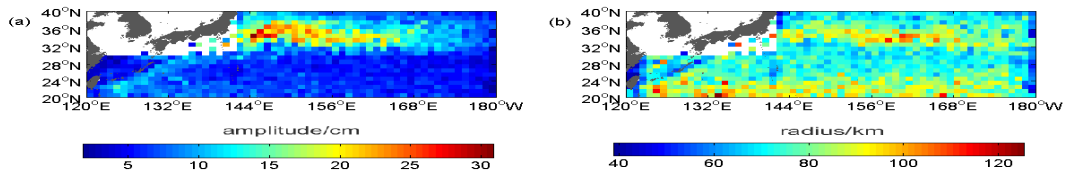

Figure 7: Spatial distribution of mean amplitude (a) and mean radius (b) of eddies

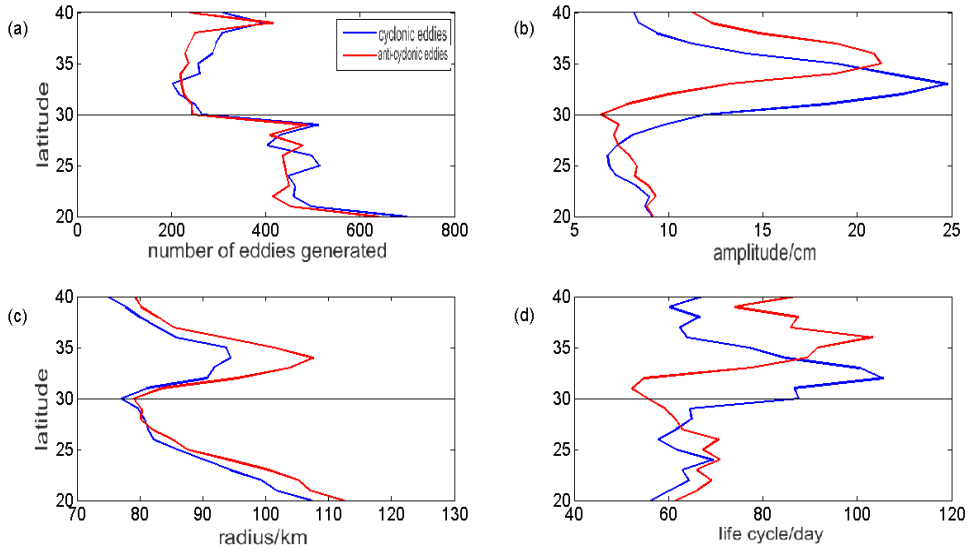

Figure 8: The meridional distributions of the number (a), amplitude (b), radius (c) and life period (d) of eddies in the study area

mesoscale eddies in the study area (zones A and B). The results show that the average amplitude of mesoscale eddies in area A is smaller than that in area B, which is consistent with the statistical results in Table 1. Chelton et al. (2011) pointed out that eddies with large amplitudes occur in sea areas with relatively unstable circulation, such as the Gulf Stream and its extension body, Kuroshio extension body, Aghales current, and Antarctic circumpolar current, etc. [3], and this result is consistent with the research results in this chapter. The average amplitude and radius of the eddies on the west side of the sea area A and B are slightly larger than those on the east side, indicating that the amplitude and radius of the eddies gradually increase during the process of westward propagation. In the study area, the radius of the eddies is relatively large in the range of 20-26°N and 30-37°N.

Figure 8 shows the meridional distribution characteristics of eddy quantity, amplitude, radius and life cycle in the study area (zones A and B). It can be seen that more eddies are generated between 20 and 22°N (more than 600), while fewer eddies are generated between 30 and 35°N. The average number of cyclonic eddies generated at each latitude is basically greater than that of anti-cyclonic eddies. The amplitude of the eddies in area B is significantly larger than that in area A, which is consistent with the results shown in Table 1 and Figure 7 (a). Among them, the amplitude of the cyclonic eddies reaches a minimum value of about 7 cm near 25°N, then gradually increases, reaches a maximum value at about 33°N, and then gradually decreases with the increase of latitude. The amplitude variation of the anti-cyclonic eddies with latitude has the same variation characteristics as that of the cyclonic eddies, but it reaches a minimum value at 30°N and a maximum value at 35°N. The radius of the eddies in the study area decreases gradually with the increase of latitude, reaching a minimum value around 30°N and a maximum value around 35°N. The radius of the anti-cyclonic eddies is larger than that of the cyclonic eddies at all latitudes. The life cycle of the eddies in area A does not change much with latitude. In the sea area of zone B, the life cycle of the cyclonic eddies is greater than that of the anti-cyclonic eddies between 30 and 34°N, while the life cycle of the cyclonic eddies is opposite between 34 and 40°N.

In order to analyze the statistical characteristics of the evolution of eddy amplitude and radius during the life cycle, the life cycle was normalized, as shown in Figure 9. As can be seen from the figure, the evolution characteristics of cyclonic eddies and anti-cyclonic eddies are similar. The amplitude of mesoscale eddies in the study area (zones A and B) generally increases gradually within 1/2 cycle after generation, reaches the extreme value basically within 1/2 cycle, and then decreases gradually. The eddies radius reaches its maximum value in 3/5 cycles after generation, and then gradually decreases, which reflects the unique variation characteristics of different eddies attributes. According to the curvature of the fitting curve, the growth rate of the radius of the eddies in the study area is always greater than the fading rate. Except for anti-cyclonic eddies in area A, the growth rate of the eddies amplitude in the study area is smaller than the fading rate. At the same time, the statistical characteristics of the amplitudes and radii of cyclonic eddies and anti-cyclonic eddies are different during their life cycle evolution. In the sea area of zone B, the amplitude of the cyclonic eddies is larger than that of the anti-cyclonic eddies, while the radius is opposite. However, in the sea area of region A, the amplitude of the cyclonic eddies is smaller than that of the anti-cyclonic eddies at about the first 1/5 of the development of the eddies, then larger than that of the anti-cyclonic eddies rom 1/5 to about 3/4, and smaller than that of the anti-cyclonic eddies from 3/4 to the extinction time. When the eddies develops to 3/10, the radius of the cyclonic eddies is smaller than that of the anti-cyclonic eddies. With the development of the life cycle, the radius of the cyclonic eddies is larger than that of the anti-cyclonic eddies until the eddies dies out.

Based on AVISO's eddies data set, Figure 10 shows the distribution histograms of eddies amplitude, radius and rotation velocity in area A and B. It can be seen that there is basically no statistical difference between cyclonic eddies and anti-cyclonic eddies in the study area (zones A and B). The amplitude, radius and rotation velocity of the eddies in zone A are mainly concentrated in 3-10 cm, 40-70 km and 15-30 cm/s, while those in zone B are 4-12 cm, 40-55 km and 18-30 cm/s. The radius distribution of eddies in area A and area B is almost the same, but the amplitude and rotation velocity of eddies in area A are significantly smaller than that in area B. Tang et al. (2019) used Rayleigh distribution function and lognormal distribution function to fit the distribution histogram of amplitude, radius and rotation velocity of eddies in STCC sea area, and concluded that the amplitude, radius and rotation velocity of eddies showed more characteristics of partial lognormal distribution

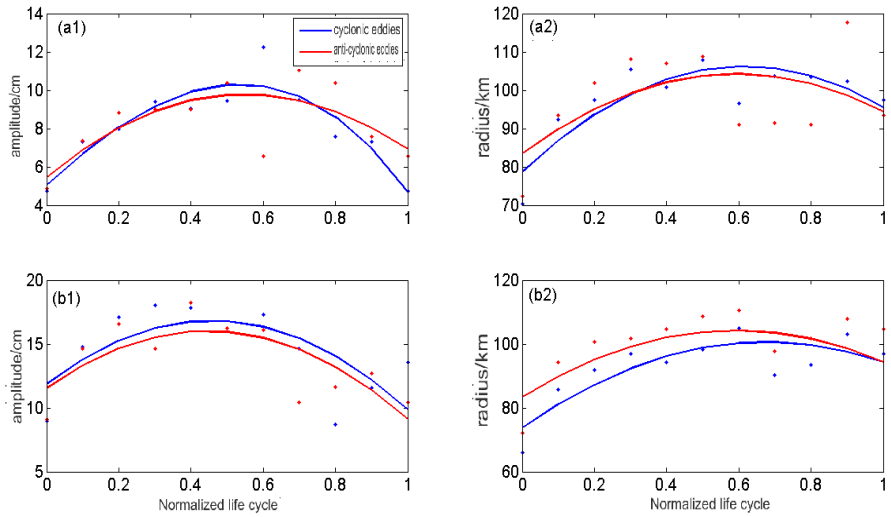

Figure 9: Evolution of eddy amplitude and radius with life period (solid line is the result of cubic polynomial fitting of corresponding parameters)

(a1) and (a2) are the sea area of A area, (b1) and (b2) are the sea area of B area

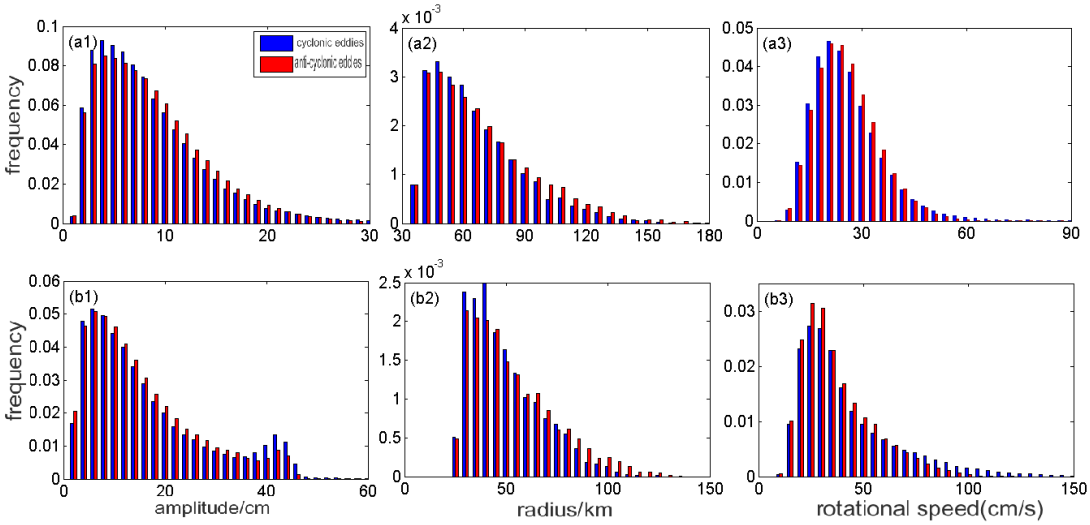

Figure 10: Histogram of the distribution of mesoscale eddy's amplitude, radius and rotation velocity in A and B sea areas

(a1), (a2) and (a3) are the sea areas of Area A, and (b1), (b2) and (b3) are the sea areas of Area B

in STCC sea area compared with Rayleigh distribution [25]. Fig. 10 (a1), (a2) and (a3) show the distribution characteristics of eddies in the sea area of STCC. It is found that the distribution of eddies does not show obvious lognormal distribution characteristics, which is inconsistent with the study of Tomball et al. (2019).

3.2 Seasonal Variation

The basic characteristics of oceanic mesoscale eddies change with the seasons. Figure 11 shows the seasonal distribution of the number, amplitude and radius of mesoscale eddies in the sea areas A and B. It can be found that the number of eddies generated in the study area (Areas A and B) is basically more in winter and spring, and less in summer and autumn. The amplitude of the eddies in the sea area of A area is larger from April to September.

Figure 12(a) shows the average number of cyclonic eddies and anti-cyclonic eddies in each month and the seasonal variation of SST in the study area (Areas A and B). It can be seen that the cyclonic eddies and anti-cyclonic eddies have similar variation characteristics (more in winter and spring, less in summer and autumn), and the number of eddies in the studied sea area has an opposite relationship with SST.

The spring with the largest number of eddies generation and the summer with the least amount were selected for comparative analysis. It can be seen from Figure 12 (b1-b3) that compared with spring, the number of eddies formation in summer in the study sea area is generally less, and the sea area with the most obvious difference in the number of eddies formation in spring and summer is at 20-30°N, 130-180°N °E. Figure 12 shows the variation of the zonal average ocean stratification index SI (defined as the average value of 0-90 m sea temperature minus the average value of 90-180 m sea temperature) in spring and summer in the study area with latitude. It can be seen that the change of ocean stratification index with latitude in spring and summer is not linear. The stratification index is lower at 26-35°N, and the corresponding number of eddies generation is more at 26-35°N (Fig. 12 (b1-b3)).

3.3 Interannual Variation

Figure 13(a) depicts the interannual variation of EKE in the study area (Areas A and B). In 1999-2004 and 2012-2014, the EKE of the eddies was significantly higher than the average level, while in 1994-1997, 2004-2011, and 2015-2017, the EKE of the eddies was significantly lower than the average level. In addition, the number, amplitude, and radius of the eddies in the study area all showed interannual variation characteristics, specifically showing that the number of eddies in 2000-2002, 2006-2008, and 2013-2015 was relatively large, while in 1994-2015 The 1998, 2003-2004, and 2009-2011 eddies had lower numbers. Both the amplitude and radius of the eddies have a periodic change of 3-4 a, the amplitude is larger in 2003 and 2005, and the radius is larger in 2005 and 2008.

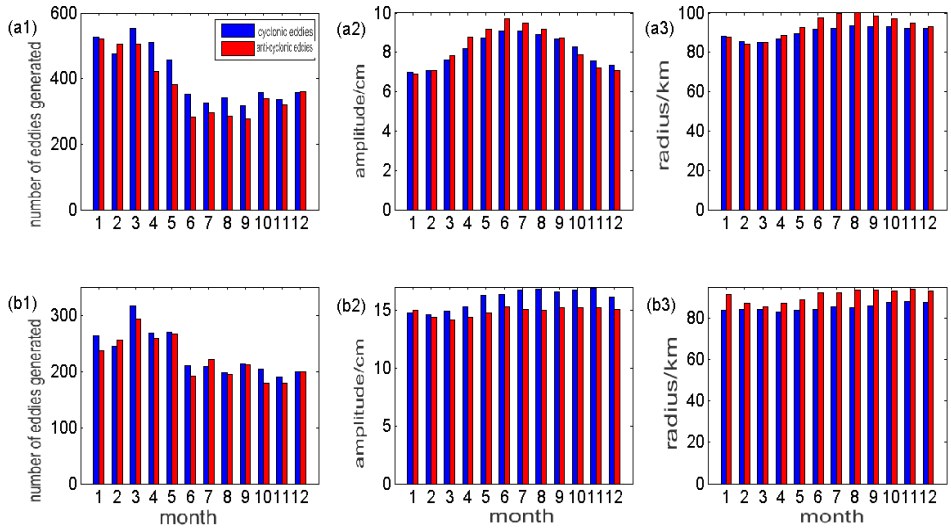

Figure 11: Seasonal distribution of mesoscale eddy's generation number, amplitude and radius in A and B sea areas

(a1), (a2), (a3) are the sea areas of Area A, and (b1), (b2), (b3) are the sea areas of Area B

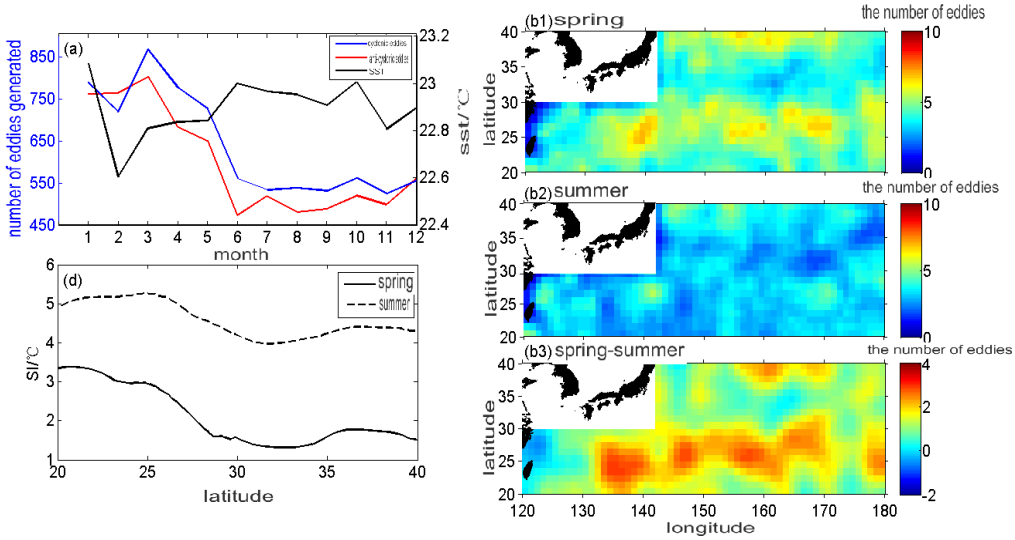

Figure 12: Seasonal variation of cyclonic eddies,anticyclonic eddies and SST (a), seasonal spatial distribution of eddies (b1-b3), and zonal mean stratification index of upper ocean (c) in the study area

(b1-b3) are the spatial distribution of the number of eddies generated in spring, summer and spring minus the number of eddies generated in summer in the study area, respectively.

The average deviation of the number of eddies generated each year is less than 8% for cyclonic eddies and less than 9% for anti-cyclonic eddies. The analysis found that the interannual variation of the number of eddies generated has a large positive correlation with PDO (the correlation coefficient of cyclonic eddies and PDO is 0.58, and the correlation coefficient of anti-cyclonic eddies is 0.64, both of which exceed the 99% confidence level).

3.4 Vertical Distribution Characteristics

Based on the identification results of the eddies and Argo data, we synthesized and studied the vertical temperature-salt-density structural sections of the eddies in the A and B sea areas. Figure 14 shows the spatial distribution of Argo numbers in cyclones and anti-cyclone eddies in the study area. It can be seen that whether it is a cyclonic eddies or an anti-cyclonic eddies, the number of Argo in the eddies in the B area is greater than that in the A area, and the Argo number density in the west side of the study area (Areas A and B) is greater than that in the east.

Figure 15 shows the vertical structure characteristics of the eddies in A and B sea areas synthesized using Argo data. It can be found that the geopotential temperature anomalies of the sea area eddies in area A are smaller than those in area B, and the depth of the anomalous extreme value of the vertical geopotential temperature of the cyclone eddies is greater than that of the sea area of area B, while the opposite is true for the anti-cyclone eddies. The vertical structure of the salinity anomaly of the eddy in the study area (Areas A and B) all presents the characteristics of "upper negative-lower positive" or "upper positive-lower negative". The "negative-positive (positive-negative)" salinity anomaly critical depth of the eddies in area A is greater than that in area B, but the salinity anomalies in the entire synthetic section are smaller than those in area B. The salinity anomaly extremum of the eddies in area A is lower than that in area B. The depth of the extreme value of the potential density anomaly of the eddies in the sea area of A area is greater than that of the sea area of B area.

4. CONCLUSION

In this paper, using the AVISO mesoscale eddy dataset from 1993 to 2020, the basic characteristics, seasonal variation and interannual variation of typical sea eddies in the Northwest Pacific Ocean were counted and analyzed. The results of the study showed that:

(1) The number of eddies (the cyclonic eddies and anti-cyclonic eddies) generated in area A sea area (STCC sea area) is greater than that in area B sea area (KE sea area), and the number of anti-cyclonic eddies generated in the two sea areas is smaller than cyclone. The eddies in the study area (Area and B) mainly moves westward, and the life cycle of the

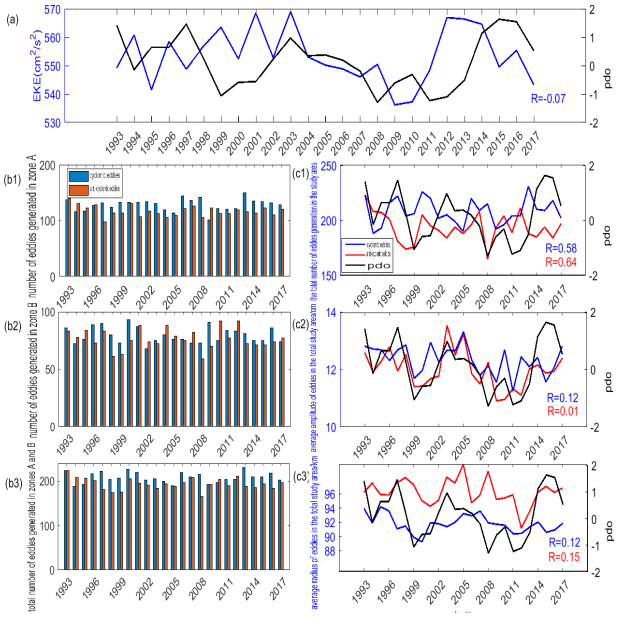

Figure 13: Interannual variation of the number of eddies (a、b1-b3) and the relationship between eddies and PDO (c1-c3)

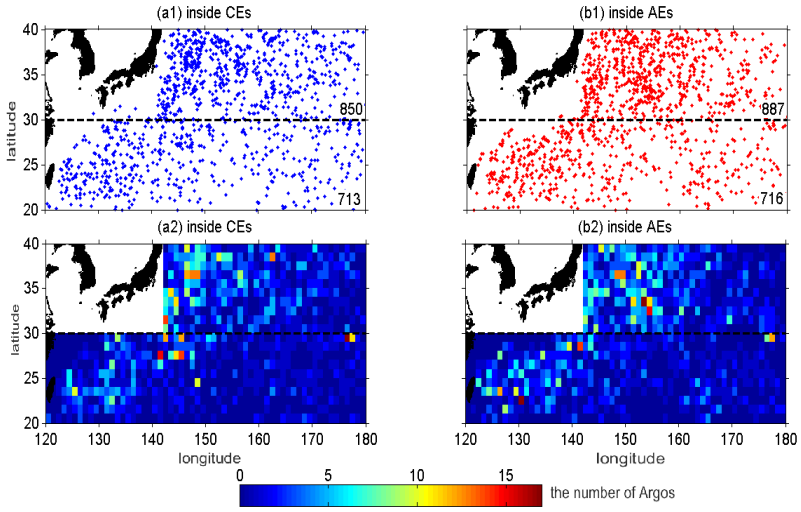

Figure 14: The spatial distribution of Argo quantity in marine cyclonic eddies and anticyclonic eddies in the study area

eddies is basically within 100 days.

(2) The number of eddies generated in the study area (Areas A and B) has obvious seasonal changes, showing the characteristics of more winter and spring and less summer and autumn, which is opposite to the seasonal change of SST. The number, amplitude and radius of eddies all show obvious interannual variation characteristics, and the interannual variation of eddies generation number is positively correlated with PDO.

(3) Synthetic analysis of the vertical structure characteristics of the sea eddies in A and B areas shows that the geopotential temperature anomaly and salinity anomaly in the synthetic section of the sea eddy in A area are smaller than those in B area, showing the opposite characteristics to the potential density anomaly. In the sea area A, the depth of the extreme value of the vertical geopotential temperature anomaly of the cyclonic eddies is greater than that of the sea area B. Contrary to the profile distribution characteristics of the salinity anomaly, the depth of the extreme value of the vertical geopotential temperature anomaly of the anti-cyclone eddies is lower than that of the B area. The regional sea area has the same profile distribution characteristics as the salinity anomaly. The salinity anomaly vertical structure of the eddy in the study area (Areas A and B) all presents the characteristics of "upper negative-lower positive" or "upper positive-lower negative", and the "negative-positive (positive-negative)" salinity anomaly critical depth is greater than that of area B.

ACKNOWLEDGEMENT

The special project for marine economy development of Guangdong Province(GDNRC[2022]31)

REFERENCES

[1] Feng, S., Li, F., Li, S. 1999. Introduction to Marine Science, Higher Education Press.

[2] Cui, W., Wang, W., Ma, Y., et al. 2017. Identification and characteristic analysis of mesoscale eddies in Northwest Pacific Ocean based on altimeter data from 1993 to 2014, Oceanographic Journal, 39, 16-28.

[3] Chelton, D. B., Schlax, M. G., Samelson, R. M. 2011. Global observations of nonlinear mesoscale eddies, Progress in Oceanography, 91(2), 167-216.

[4] Chaigneau, A., Le Texier, M., Eldin, G., et al. 2011. Vertical structure of mesoscale eddies in the eastern South Pacific Ocean: A composite analysis from altimetry and Argo profiling floats, Journal of Geophysical Research: Oceans, 116(C11025), 1-16.

[5] Babu, M. T., Prasanna Kumar, S. Rao, D. P. 1991. A subsurface cyclonic eddy in the Bay of Bengal, Journal of Marine Research, 49(3), 403-410.

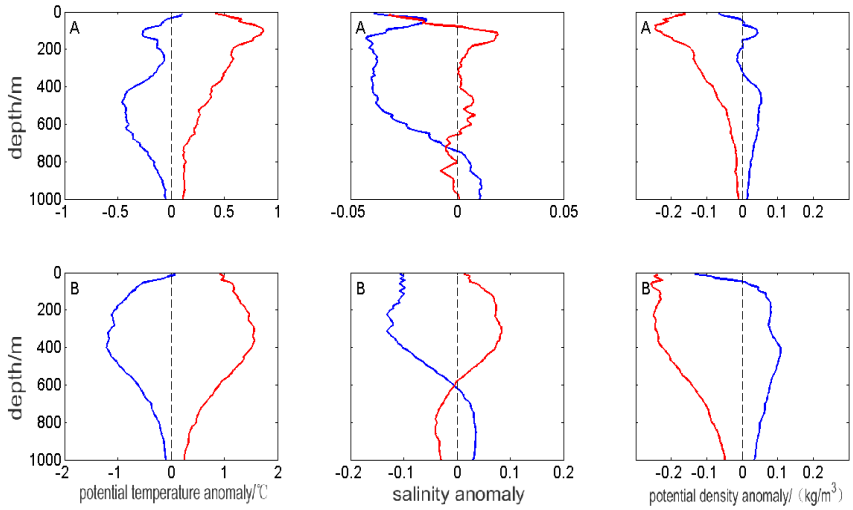

Figure 15: Abnormal profile of potential temperature, salinity and potential density in A and B sea areas

[6] Wang, G. H., Su, J. L. Qi, Y. Q. 2005. Advances in studying mesoscale eddies in South China Sea, Advances in Earth Science, 20, 882-886.

[7] Chaigneau, A., Gizolme, A. Grados, C. 2008. Mesoscale eddies off Peru in altimeter records: identification algorithms and eddy spatio-temporal patterns, Progress in Oceanography, 30, 106-119.

[8] Stammer, D. 1997. Global characteristics of ocean variability estimated from regional TOPEX/Poseidon altimeter measurements, Journal of Physical Oceanography, 27(8), 1743-1769.

[9] Stammer, D. 1998. On eddy characteristics, eddy transports, and mean flow properties, Journal of Physical Oceanography, 28(4), 727-739.

[10] Qiu, B., Chen, S. M. 2005. Eddy-induced heat transport in the subtropical North Pacific from Argo, TMI, and altimetry measurements, Journal of Physical Oceanography, 35(4), 458-473.

[11] Chen, G. X., Hou, Y. J., Chu, X. Q. 2011. Mesoscale eddies in the South China Sea: Mean properties, spatiotemporal variability, and impact on thermohaline structure, Journal of Geophysical Research: Oceans, 116(C6), C06018.

[12] Chen, G. X., Gan, J. P., Xie, Q. et al. 2012. Eddy heat and salt transports in the South China Sea and their seasonal modulations, Journal of Geophysical Research: Oceans, 117(C5), C05021.

[13] Liu, F. F., Chen, C. Q., Tang, S. L. et al. 2011. Retrieval of chlorophy ll a concentration from a fluorescence enveloped area using hyperspectral data, International Journal of Remote Sensing, 32(13), 3611-3623.

[14] Dong, C. M., Nencioli, F., Liu, Y. et al. 2011. An automated approach to detect oceanic eddies from satellite remotely sensed sea surface temperature data, IEEE Geoscience and Remote Sensing Letters, 8(6), 1055-1059.

[15] Wang, Ru., Li, Haiyan., Meng, L. 2019. Study on energy characteristics of mesoscale eddies in the North Pacific Kuroshio extension area and subtropical countercurrent area, Oceanographic Journal, 41(11), 1-14.

[16] Qiu, B., Kelly, K. A., Joyce, T. M. 1991. Mean flow and variability in the Kuroshio Extension from Geosat altimetry data, Journal of Geophysical Research: Oceans, 96(C10), 18491-18507.

[17] Kobashi, F., Kawamura, H. 2002. Seasonal variation and instability nature of the North Pacific Subtropical Countercurrent and the Hawaiian Lee Countercurrent, Journal of Geophysical Research: Oceans, 107(C11), 6-1:6-18.

[18] Ebuchi, N., Hanawa, K. 2001. Trajectory of Mesoscale Eddies in the Kuroshio Recirculation Region, Journal of Oceanography, 57(4), 471-480.

[19] Sasaki, Y. N. Minobe, S. 2015. Climatological mean features and interannual to decadal variability of ring formations in the Kuroshio Extension Region, Journal of Oceanography, 71(5), 499-509.

[20] Ding, Y., Jing, C., Qiu, Y. 2019. Spatiotemporal analysis of the shedding eddies in the area of the Kuroshio extension, Oceanographic Journal, 41(5), 47-58.

[21] Qiu, B. 1999. Seasonal Eddy Field Modulation of the North Pacific Subtropical Countercurrent: TOPEX/Poseidon Observations and Theory, Journal of physical oceanography, 29, 2471-2486.

[22] Qiu, B. Chen, S. M. 2014. Seasonal Mesoscale and Submesoscale Eddy Variability along the North Pacific Subtropical Countercurrent, Journal of physical oceanography, 44, 3079-3097.

[23] Li, H., Xu, Y. 2017. Seasonal variation and mechanism of eddy kinetic energy spectrum in subtropical countercurrent area of North Pacific Ocean, Ocean and Limnology, 48(5), 932-943.

[24] Liu, Y., Dong, C. M., Guan, Y. P. et al. 2012. Eddy analysis in the subtropical zonal band of the North Pacific Ocean, Deep Sea Research Part I: Oceanographic Research Papers, 68, 54-67.

[25] Tang, B., Hou, Y., Yin, Y., et al. 2019. Statistical characteristics and distribution of mesoscale eddies in the North Pacific subtropical countercurrent area, Ocean and Limnology, 50, 937-947.